



RESEARCH ARTICLE

Novel analysis of the size and orientation dependent resonance phenomenon of the microstrip line coupled complementary split-ring resonator

Nilesh K. Tiwari | Abhishek Sharma | Surya P. Singh | M. Jaleel Akhtar | Animesh Biswas

Department of Electrical Engineering,
Indian Institute of Technology Kanpur,
Kanpur, Uttar Pradesh, India

Correspondence

Nilesh K. Tiwari, Department of Electrical
Engineering, Indian Institute of
Technology Kanpur, Kanpur, Uttar
Pradesh, India.
Email: nileshkt85@gmail.com

Abstract

The purpose of this article is to provide a comprehensive investigation on the resonance phenomenon of microstrip line coupled complementary split-ring resonator (CSRR) with different orientation and relative size. It is shown that when the relative size of the CSRR is smaller than the host line, the CSRR with its slit oriented orthogonal to the line axis will not excite effectively and show weak resonance behavior. However, when the slit is positioned along the line axis, the cross-polarization effect comes into play, which excites the CSRR through the mixed coupling. To ensure the correctness, several numerical simulations are carried out for different substrate height and relative permittivity. Finally, a prototype is fabricated and measured for the experimental validation.

KEYWORDS

complementary split-ring resonator, split-ring resonator, microstrip line

1 | INTRODUCTION

The past decade have seen colossal growth in design and investigation of the artificial materials known as metamaterials to control the electromagnetic properties. These type of materials show exotic electromagnetic phenomenon such as inversion of Snell's law, inversion of Doppler effect, focusing, and so forth.¹ To realize these type of materials split-ring resonator (SRR) and complementary split-ring resonator (CSRR) have been proposed as basic entities (unit cells),^{1,2} and these electrically small resonators have been applied to design several novel microwave circuits and antennas.^{1,3-7} Thus, the interaction of these resonators with the electromagnetic wave is very crucial for the understanding of their behavior. From the earlier investigations,⁸⁻¹⁰ it has been concluded that the CSRR/SRR can be considered as an electric/magnetic dipole that can be excited using an axial electric/

magnetic field. Moreover, the effect of CSRR and SRR orientation relative to the host transmission line has been investigated in Reference 11, and it has been shown that when the slit of CSRR/SRR are aligned along the line axis, the cross-polarization effect arises and due to which these resonators can be excited through both electric and magnetic field.

Consider two orientation for the microstrip coupled CSRR: (a) O-CSRR: when the slit is oriented orthogonally to the host line and (b) I-CSRR: when the slit is oriented along the longitudinal axis of the host line. Most of the CSRR based structures analyzed in the past few years have considered the relatively larger CSRR with respect to the width of host line, that is, $W_1/a < 1$, where W_1 is the microstrip line width and a is outer dimension of CSRR ring. For $W_1/a < 1$, the CSRR in both the configuration, that is, O-CSRR, and I-CSRR can be excited effectively. The earlier investigation of I-CSRR reveals that due

the presence of geometrical asymmetry the CSRR can be excited using mixed coupling (both electric and magnetic coupling).¹¹ Extending this further, the investigation in this article reveals that the resonant frequency and 3-dB fractional bandwidth (FBW) of CSRR in both the configurations is slightly different, which is basically due to the different excitation mechanism.

Now, the question arises what will happen when the relative size of CSRR with respect to the host line become small or comparable, that is, when the aspect ratio W_1/a becomes greater than unity. To the authors' best knowledge this kind of investigation has not been done previously, which motivates the authors to provide a more comprehensive investigation on the orientation of CSRR for $W_1/a > 1$. Our finding shows that when the size of CSRR is smaller than the width of microstrip line, then the O-CSRR do not exhibit good resonance due to weak electric coupling whereas the I-CSRR configuration show prominent resonant phenomenon due to mixed coupling where the magnetic coupling dominates over the electric coupling. This anomaly is supported by extensive numerical simulations, field distribution, and experimental verification. The following points mainly describes the novelty of the proposed work:

1. First of all, a comprehensive analysis of microstrip line coupled arbitrary orientated CSRR structure corresponding to its various size especially when its size is relatively smaller than the microstrip line width, that is, $W_1/a > 1$ is first time demonstrated in this work.
2. The relatively higher insertion loss generation of the ICSRR structure over the OCSRR structure for $W_1/a > 1$ is explicitly reported which is not yet available in the literature.
3. In this work, it is shown that the proposed ICSRR topology helps to develop the high frequency compact resonating structures including the dielectric sensor, which was not possible with the conventional OCSRR topology.
4. The effect of substrate height for wide and moderately wide microstrip line on the resonant behavior of ICSRR and OCSRR structure corresponding to various possible combination of W_1/a , is first time analyzed in detail.
5. A simplified equivalent circuit topology with the corresponding values of the optimized parameters is explicitly developed for the ICSRR structure to advocate its cross-coupling mechanism for W_1/a .

2 | ANALYSIS OF O-CSRR AND I-CSRR STRUCTURES

The numerical analysis of the I-CSRR and O-CSRR structures is carried out using the frequency domain solver of

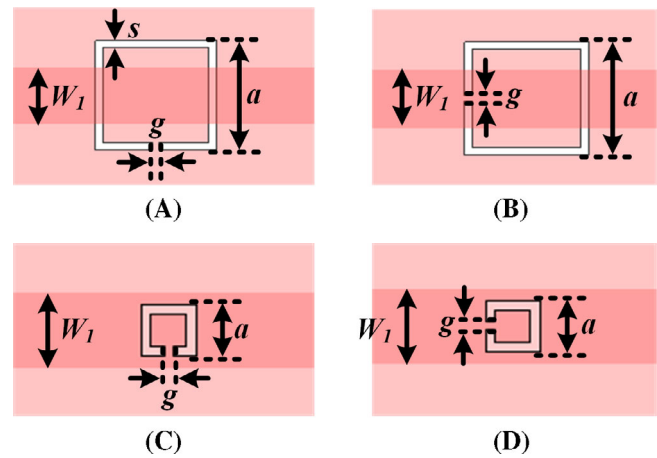


FIGURE 1 CSRR coupled to microstrip line: A, O-CSRR with $W_1/a < 1$; B, I-CSRR with $W_1/a < 1$; C, O-CSRR with $W_1/a > 1$; D, I-CSRR with $W_1/a > 1$ (geometrical parameters: $g = 0.25$ mm and $s = 0.3$ mm)

the full wave electromagnetic solver-CST MWS with incorporating the open boundary conditions and the customized Tetrahedron mesh setting to obtain the proper convergence of the simulation results. Figure 1 shows the numerical model of O-CSRR and I-CSRR configuration for $W_1/a < 1$ and $W_1/a > 1$. The microstrip line is printed on the top side of the substrate whereas the CSRR is etched on the ground plane of the microstrip line. The analysis starts off with $W_1/a < 1$, where the dimensions of the CSRR are chosen as $a = 12.9$, $s = 0.3$, $g = 0.25$ (all are in millimeters) and the ratio W_1/h is kept constant corresponding to 50Ω . For example, $W_1 = 5.1$ mm, and 2.55 mm for $h = 1.6$ mm, and 0.8 mm, respectively corresponding to 50Ω wide microstrip line designed on TLY-5 substrate whereas $W_1 = 3.2$ mm, and 1.6 mm for $h = 1.6$ mm, and 0.8 mm, respectively corresponding to 50Ω narrow microstrip line designed on the FR-4 substrate. For this configuration, it has been observed in the past both the CSRR configuration, that is, O-CSRR and I-CSRR get excited effectively. The former (OCSRR) gets excited only through the electric coupling whereas the latter (OCSRR) gets excited through the mixed coupling, that is, by both electric and magnetic coupling. Thus, for $W_1/a < 1$ the excitation of CSRR is negligibly sensitive to its rotation with respect to the host line. Here, it is also worth mentioning that the resonant frequency and 3-dB FBW for both configurations are slightly different which is due to their associated excitation mechanism as described in later section.

Next, the detailed analysis is carried out for O-CSRR and ICSRR having different W_1/a ratio for the particular substrate thickness and relative permittivity. Here, the two cases are considered, that is, (a) wide microstrip line

($W_1/h > 3$) and (b) moderately wide microstrip line ($W_1/h < 3$).¹²

2.1 | Numerical analysis of I-CSRR and O-CSRR coupled to wide microstrip line ($W_1/h > 3$)

A wide microstrip line having width $W_1 = 5.1$ mm is designed on TLY5 substrate of thickness $h = 1.6$ mm and dielectric constant of 2.2. A CSRR having dimensional parameters a , g and s is etched on the ground plane of the host microstrip line. The values of s and g are taken as 0.3 mm and 0.25 mm, respectively and the value of a is varied to generate the plot of S_{21} . Figure 2 shows the S_{21} for different values of W_1/a corresponding to both O-CSRR and I-CSRR configurations. From the figure, it can be clearly observed that the weak resonance (which here is defined for $|S_{21}| > -10$ dB) prevails in the OCSRR for certain values of W_1/a , which in this case is found to be greater than 1.4. This basically means that the O-CSRR structure is not driven properly for the values of W_1/a

$a > 1.4$ due to the weak electric coupling. In the present situation, the value $W_1/a = 1.4$ can be considered as a transition value (ζ) from strong resonance to weak resonance region. However, the CSRR in the I-CSRR configuration get excited even for $W_1/a > 1.4$. This is due to the fact that I-CSRR configuration gives rise to the cross-polarization phenomenon and in this case the CSRR get excited through mixed coupling having the dominance of magnetic coupling. This is illustrated in the subsequent section using the field distribution plot.

To corroborate the proposed finding the analysis is also carried out for different substrate thickness. Figures 3 and 4 show the S_{21} for different values of W_1/a for $h = 1.2$ mm and $h = 0.8$ mm, respectively. Here, the width of microstrip line is taken as 3.7 mm, and, 2.55 mm, respectively, to maintain the wide microstrip line criteria and 50 Ω impedance. In this case, the same argument as discussed previously can be given for both the O-CSRR and I-CSRR structures. The difference is only in the transition region which in this case is defined at $\zeta = 1.37$, and $\zeta = 1.34$, respectively, which might be due to the difference in the h , and a , in both the cases.

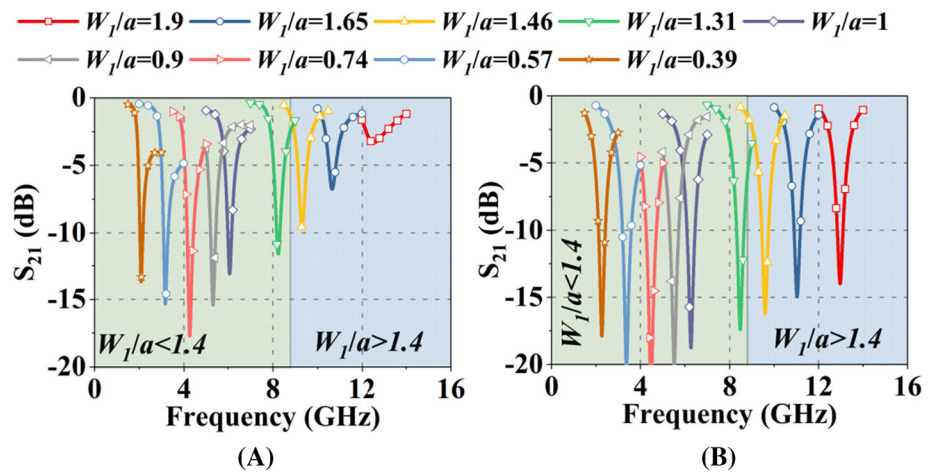


FIGURE 2 Numerically generated transmission coefficient (S_{21}) for different values of W_1/a : A, O-CSRR; B, I-CSRR

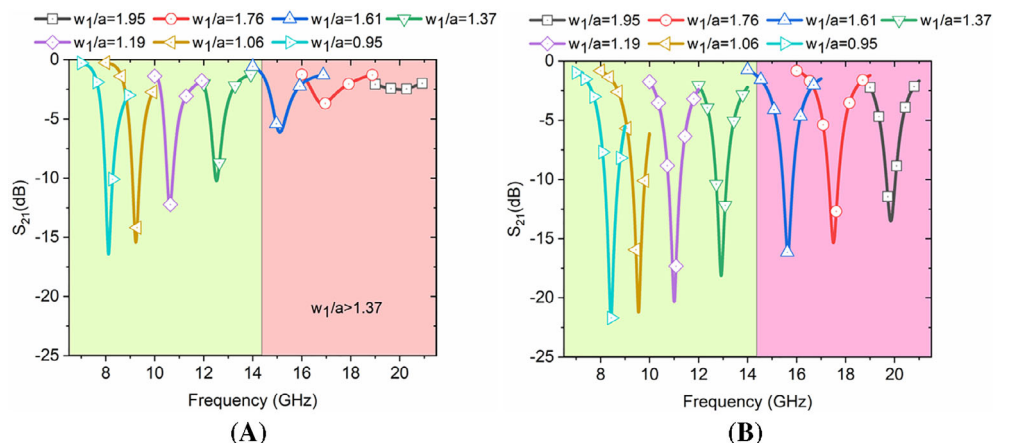


FIGURE 3 Numerically generated transmission coefficient (S_{21}) for different values of W_1/a : A, O-CSRR; B, I-CSRR, corresponding to the $h = 1.2$ mm

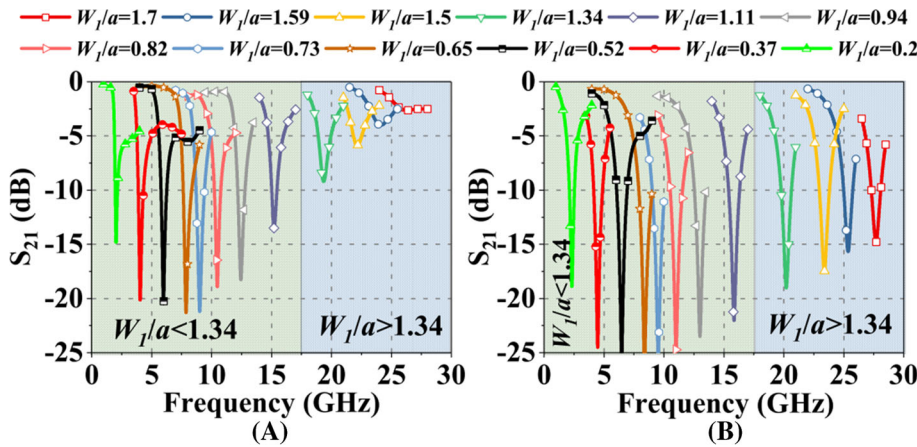


FIGURE 4 Numerically generated transmission coefficient (S_{21}) for different values of W_1/a : A, O-CSRR; B, I-CSRR, corresponding to the $h = 0.8$ mm

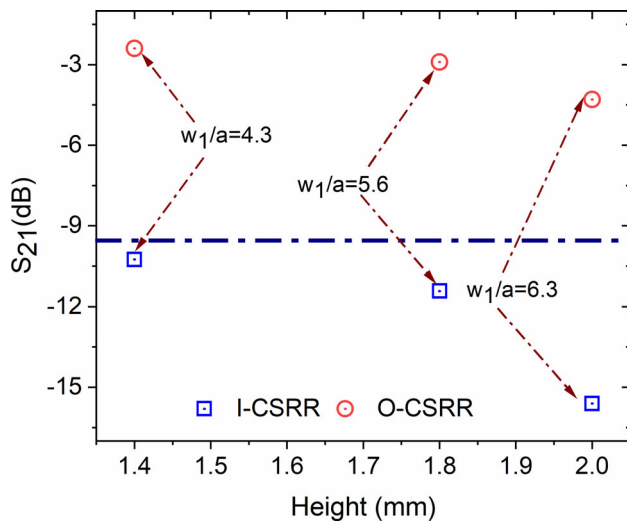


FIGURE 5 Numerically generated transmission coefficient (S_{21}) for different values of substrate height h corresponding to the various values of W_1/a

The plot of insertion loss at the resonant frequency of the ICSRR, and OCSRR structures corresponding to the various substrate heights are provided in Figure 5. From this figure, it can be ascertained that the ICSRR/OCSRR structures produces the strong/ weak resonances, respectively for different values of substrate height for $W_1/a > 1$. From this figure, it can clearly be observed that the ICSRR structure always produces the good insertion loss (>10 dB) whereas OCSRR results the generation of poor insertion loss irrespective of the substrate height value when $W_1/a > 1$. Hence, it can be concluded that the proposed finding is valid irrespective of substrate thickness keeping the aspect ratio W_1/h such that the microstrip line bears 50Ω impedance.

To gain more confidence on the proposed findings, we have also analyzed the same structures for the case of moderately wide microstrip line ($W_1/h < 3$).

2.2 | Numerical analysis of I-CSRR and O-CSRR coupled to moderately wide microstrip line ($W_1/h < 3$)

In this analysis, the microstrip line is printed on FR4 substrate having dielectric constant of 4.3. The width of the microstrip line is taken as 3.2 and 1.6 mm corresponding to $h = 1.6$ and $h = 0.8$ mm, respectively. Figure 6 shows the S_{21} for different values of W_1/a . From the figure, it can be inferred that even for different value of relative permittivity, the O-CSRR and I-CSRR shows similar resonance phenomenon as predicted for $\epsilon_r = 2.2$. However, in this case the transition from strong to weak resonance take place at $\zeta = 1.3$ and $\zeta = 1.15$ for $h = 1.6$ mm and $h = 0.8$ mm, respectively.

In summary, it is concluded that the proposed findings regarding the orientation and relative size of CSRR are valid for different substrate thickness and relative permittivity. In all the cases, the resonance behavior remains similar for both the O-CSRR and I-CSRR configurations except the transition value ζ . The slight difference in the ζ can mainly be attributed to the difference in absolute value of a , h , and ϵ_r .

3 | RESULTS AND DISCUSSIONS

3.1 | Field distribution

To provide the clear interpretation about the specific coupling mechanism associated with the ICSRR and OCSRR structure, the plot of unperturbed and perturbed electric and magnetic fields in the YZ-plane are now included as shown in Figures 7 and 8. Here it is to be noted that the magnetic field lines of host microstrip line lies parallel to the symmetry wall of the CSRR structure resulting to the negligible magnetic coupling whereas small etched region corresponding to $W_1/a > 1$ may also not produces the significant electric field perturbation. This fact can

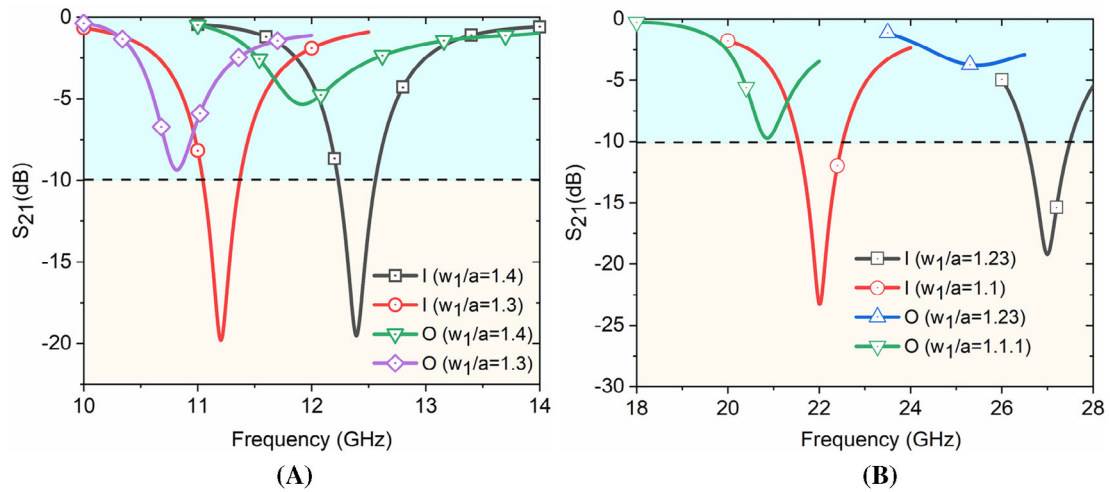


FIGURE 6 Numerically generated transmission coefficient (S_{21}) for different values of W_1/a for (A) $h = 1.6$ mm; (B) $h = 0.8$ mm. I in legend represent I-CSRR and O- in legend represents O-CSRR

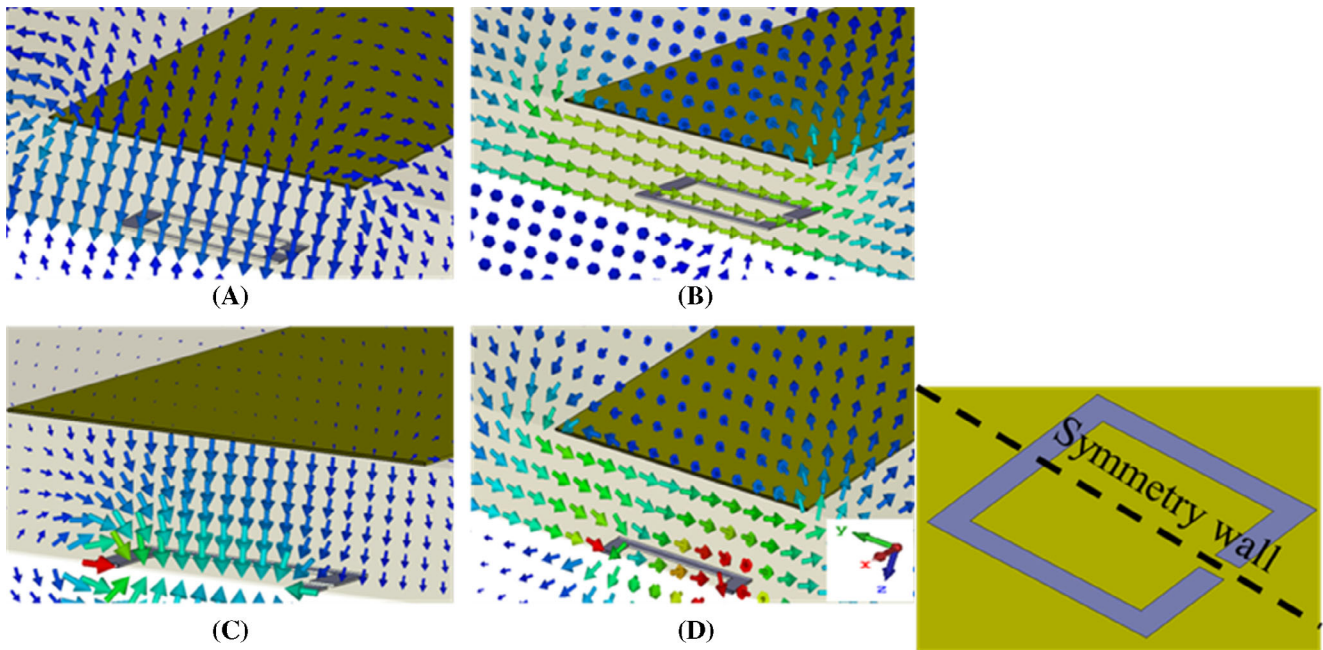


FIGURE 7 Plot of electric and magnetic field of the microstrip line along YZ-plane at resonant frequency of the O-CSRR structure when $W_1/a > 1$ corresponding to the (A) unperturbed electric field far from the O-CSRR structure, (B) perturbed electric field over the O-CSRR region, (C) unperturbed magnetic field far from the O-CSRR structure, (D) perturbed magnetic field over the O-CSRR region

clearly be visualized from Figure 7, where the perturbed and unperturbed field appears nearly same for the OCSRR structure with $W_1/a > 1$. This basically means that merely the presence of pure electric coupling might not prove to be viable option to produce the proper excitation of the ground etched OCSRR structure with $W_1/a > 1$. On the other hand, for the ICSRR structure, the electric coupling remains nearly similar to that of the OCSRR structure (negligibly smaller for $W_1/a > 1$) due to the presence of similar etched area perpendicular to the

host microstrip line. However, for the ICSRR structure, the magnetic field line becomes perpendicular to its symmetry walls (Figure 8) results to the generation of significant magnetic coupling. Therefore, the electrically and magnetically excited ICSRR structure may produces the significant perturbation of the electric and magnetic field of the microstrip line, refer Figure 8 resulting to generation of good insertion loss at its resonant frequency.

Now, plot of the magnetic field and electric field distribution in O-CSRR and I-CSRR structure for $W_1/a > 1$

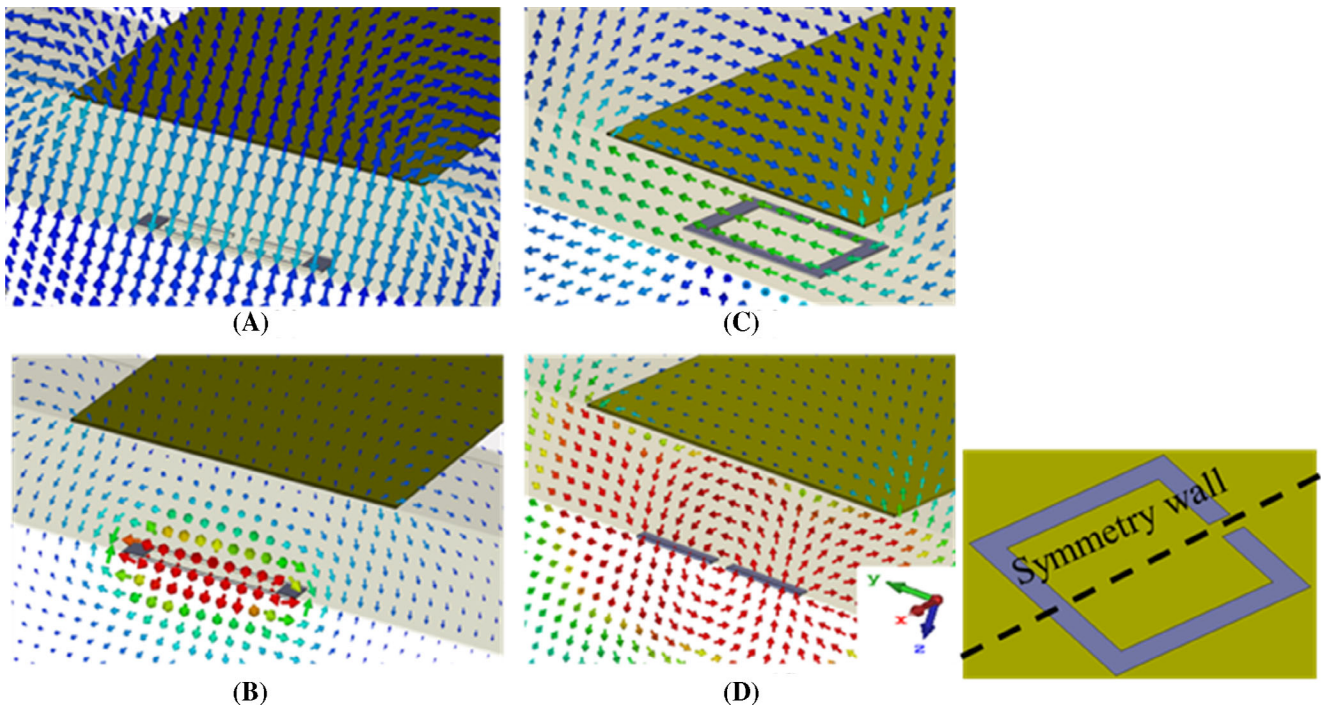


FIGURE 8 Plot of electric and magnetic field of the microstrip line along YZ-plane at resonant frequency of the I-CSRR structure when $W_1/a > 1$ corresponding to the (A) unperturbed electric field far from the I-CSRR structure, (B) perturbed electric field over the I-CSRR region, (C) unperturbed magnetic field far from the I-CSRR structure, (D) perturbed magnetic field over the I-CSRR region

in the XY-plane, at corresponding resonant frequencies are shown in Figure 9A,B and Figure 9C,D, respectively to show the localization of field lines in the resonators at their resonant frequency. From the figure, it is observed that a strong magnetic field orthogonal to the symmetry plane is localized in I-CSRR configuration as compared to O-CSRR. Similarly, the higher electric field lines remains localized in the etched region of the ICSRR structure than that of the OCSRR structure at corresponding resonant frequencies. This is mainly due to the presence of the cross-polarization effect in I-CSRR. Although the electric coupling is present in both the cases, however, due to its weak nature, the O-CSRR is excited weakly whereas the presence of the additional magnetic coupling in I-CSRR excites the structure effectively which is quite evident from the field lines shown in the YZ-plane, Figures 7 and 8. Finally, the absolute value of the electric field localized in the OCSRR and ICSRR structures is shown in Figure 10 to visualize the intensity of strong field localization associated with the ICSRR structure than that of the OCSRR counterpart. This figure clearly demonstrate the presence of strong localized electric field in the ICSRR structure unlikely the OCSRR structure. The aforementioned field analysis of the resonators shown in Figures 7 and 8, thus, depicts that the ICSRR structure gets excited by the magnetic field line of the microstrip line which results to the significant

perturbation and hence localization of the fields at the resonant frequency unlikely the poorly excited OCSRR structure, as depicted in Figure 9.

3.2 | Equivalent circuit

The O-CSRR structure possesses geometrical symmetry with respect to the excitation ports whereas the I-CSRR is asymmetric configuration. This asymmetry in I-CSRR yields the cross-polarization effect which result in the excitation of CSRR in this particular configuration using the mixed coupling. The lumped equivalent circuit model of both O-CSRR and I-CSRR is depicted in Figure 11A,B, respectively. The O-CSRR configuration can be driven by the axial electric field, that is, it can only be excited using electric coupling, which can represented by coupling capacitance, C_C in the equivalent circuit model.¹¹ However, when the CSRR is rotated by 90° to realize I-CSRR configuration, a non-negligible component of the magnetic field orthogonal to the symmetry plane of the CSRR exists, and hence both magnetic and electric coupling must be considered in this case.¹¹ To introduce the effect of magnetic coupling an extra coupling inductance L_C is added parallel with C_C in the lumped equivalent model. This inductance reduces the overall inductance thereby increases the

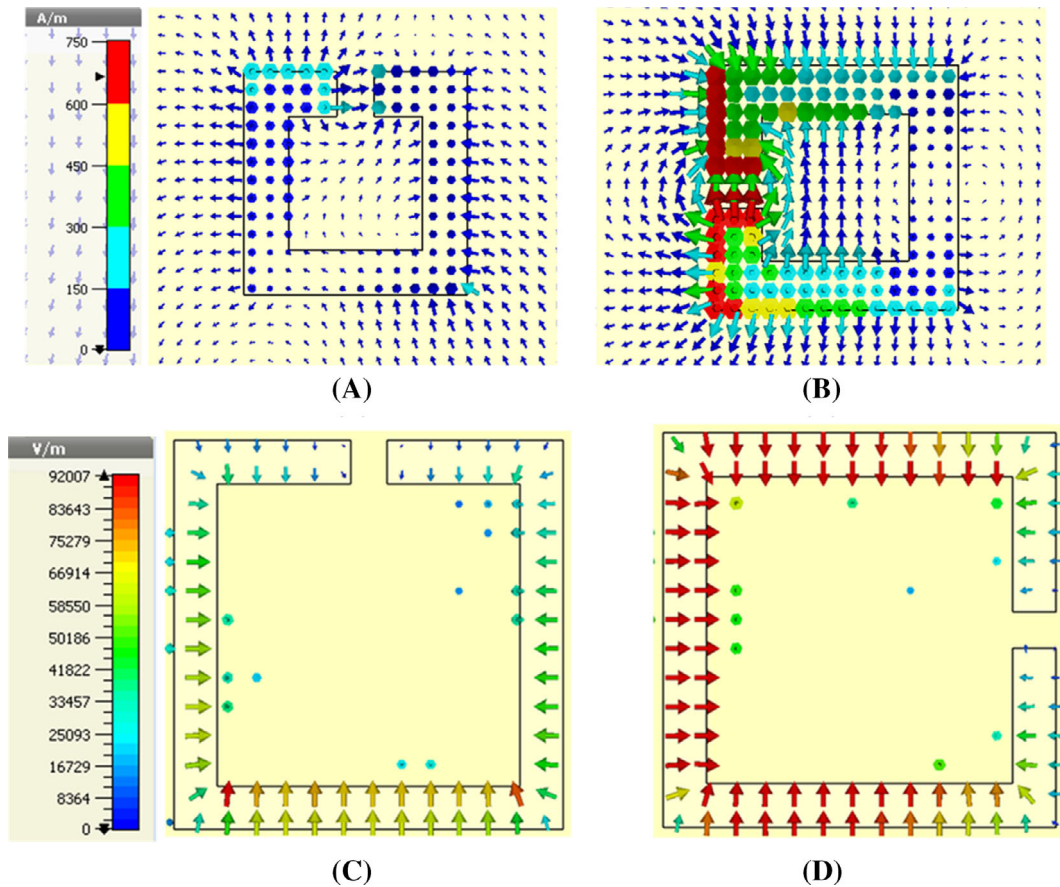


FIGURE 9 Numerically generated Magnetic field line at the resonant frequency of the (A) O-CSRR and (B) I-CSRR, and electric field line of the (C) O-CSRR and (D) I-CSRR. This plot is for the aspect ratio W_1/a greater than unity

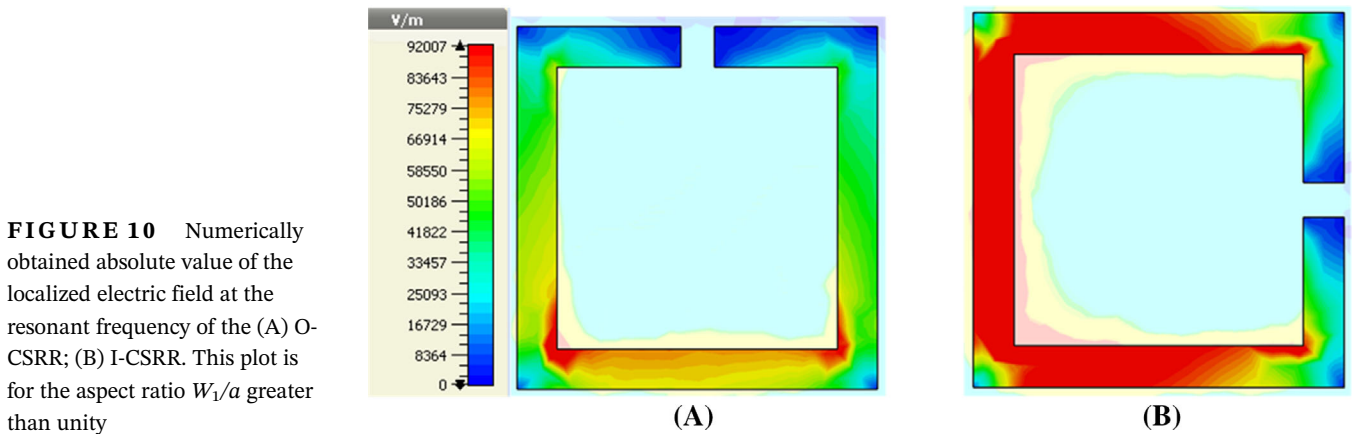


FIGURE 10 Numerically obtained absolute value of the localized electric field at the resonant frequency of the (A) O-CSRR; (B) I-CSRR. This plot is for the aspect ratio W_1/a greater than unity

resonant frequency slightly than that of the OCSRR structures shown in Figure 2.

For the case when the size of CSRR is relatively larger than the microstrip line, it gets effectively excited through the electric coupling irrespective of its orientation. However, when the relative size become smaller than the host line, the electric coupling becomes weak and therefore, the excitation of CSRR become difficult which can be well understood from the equivalent circuit

model of O-CSRR where only the electric coupling is present. The weak electric coupling yields smaller value of C_C that can be neglected in both the configurations. This result in the weak excitation of O-CSRR, however, the presence of an extra inductance (due to the cross-polarization effect) in case of I-CSRR helps it to get excited effectively through magneto-electric coupling.

The equivalent circuit model of the OCSRR structure mainly describes the electrically coupled parallel L_C

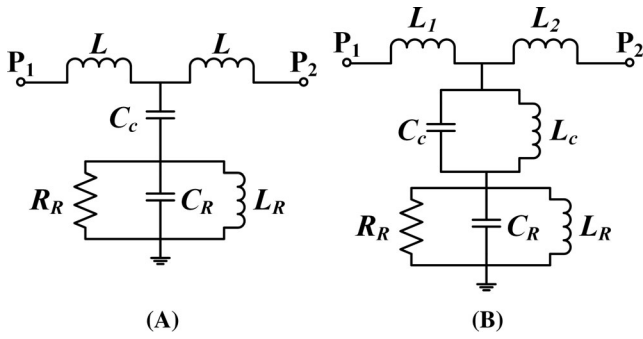


FIGURE 11 Lumped equivalent circuit model for (A) O-CSRR and (B) I-CSRR

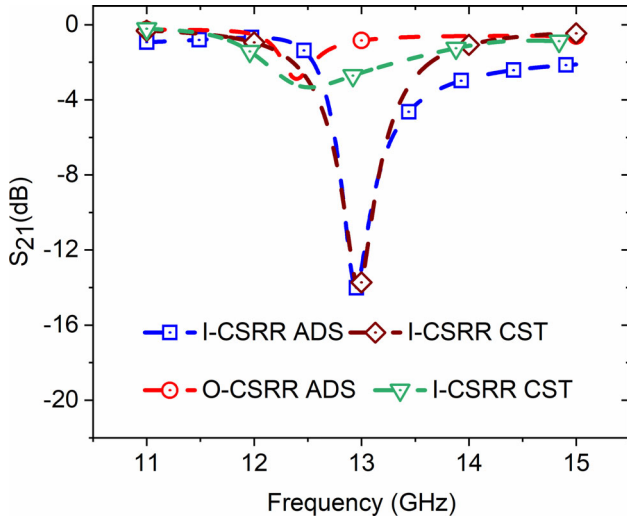


FIGURE 12 The transmission coefficient (S_{21}), generated using the CST and ADS simulation software for O-CSRR, I-CSRR structures

resonator whereas the ICSRR topology is depicted as the mixed coupled (electric and magnetic) parallel L_C resonating element. The resonant frequency of the OCSRR and ICSRR structures thus can be given as (1) at their corresponding resonant frequencies.

$$\begin{aligned} f_{rI} &= \frac{P_I}{2\pi\sqrt{(L_C || L_R)(C_C + C_R)}} \\ f_{rO} &= \frac{P_O}{2\pi\sqrt{(L_R)(C_C + C_R)}} \end{aligned} \quad (1)$$

The CST generated plots of the transmission coefficient at the resonant frequency of the OCSRR and ICSRR structures are compared accordingly with the corresponding ADS circuit simulator generated S-parameters as shown in Figure 12 corresponding to the optimized values of the main circuit parameters. From

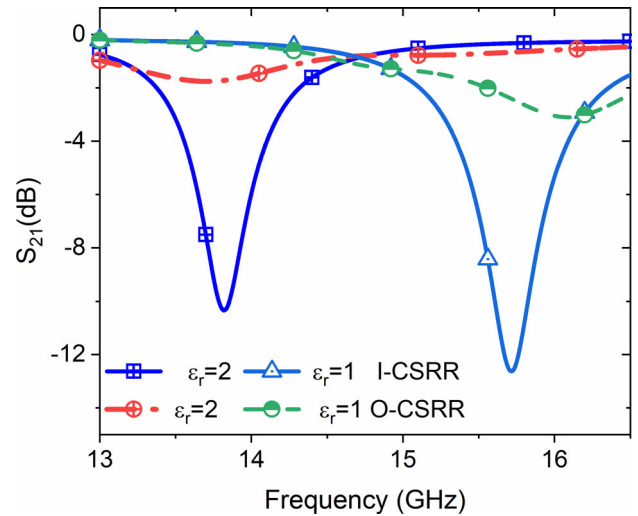


FIGURE 13 High frequency dielectric sensing feature of the proposed ICSRR topology over the conventional OCSRR topology

this figure, it can be noticed that the S-parameters generated using both the approaches are in good agreement with each other. The final value of the optimized parameter in present situation, which primary governs the resonant characteristic of the ground etched OCSRR and ICSRR resonators are $L_R = 0.203$ nH, 0.228 nH, $C_R = 0.759$ pF, 0.792 pF, $C_C = 0.057$ pF, 0.05 pF, respectively whereas the value of coupling inductance (L_C) corresponding to ICSRR resonator founds to be 0.813 nH. From these set of values, it can clearly be ascertained that the coupling capacitance C_C bears a quite small value and hence the OCSRR structure leads to poor excitation. On contrary, ICSRR structure possesses the strong resonant behavior (Figure 12) due to the presence of additional magnetic coupling (L_C) as shown in Figure 11.

3.3 | High frequency dielectric sensing attributes of the ICSRR topology

The high frequency dielectric sensing attribute of the proposed ICSRR topology for $W_1/a > 1$ is described here to appreciate its distinct gain over the conventional OCSRR topology. Figure 13 shows the transmission coefficient response of the ICSRR and OCSRR structures at the resonant frequency of 15.6 GHz for $W_1/a > 1$. From this figure, it can be seen that the OCSRR structure does not produce the substantial insertion loss at its unloaded resonant frequency due to its poor coupling. Therefore, loading of dielectric sample with $\epsilon_r = 2$ could not reflect the noticeable resonant frequency under observation. However, from the unloaded S_{21} plot of the ICSRR structure, it can be seen that the ICSRR structure might produce the substantial insertion loss at the corresponding

resonant frequency. The loading of sample with $\epsilon_r = 2$ thus results to the generation of certain noticeable change in the resonant frequency as shown in Figure 13. Therefore, it can be said that the ICSRR structure can effectively be used to develop the compact high frequency (which is in present situation is 15.6 GHz) dielectric sensor unlikely the conventional OCSRR structure. It is might be due to this reason, most of the OCSRR loaded sensors are mainly reported at the low operating frequency.¹⁻⁵

The basic principle of dielectric sensing mechanism associated with the ICSRR topology may qualitatively being expressed using (2). This relation states that the resonant frequency of the ICSRR structures will get decreased with an increase in the dielectric constant of the samples (ϵ_r).

$$f_{rI} = \frac{P_I}{2\pi\sqrt{(L_C||L_R)(C_C + C_R)}} \quad (2)$$

$$= \frac{P_I}{2\pi\sqrt{(L_C||L_R)(C_C + C_{R0} \cdot \epsilon_{rS})}}$$

3.4 | Experimental results

For the experimental verification both the configuration are built on 1.6 mm thick TLY5 substrate having relative permittivity of 2.2. The geometrical dimensions are: $a = 2.7$ mm, $s = 0.3$ mm, $g = 0.25$ mm, and $W_1 = 5.1$ mm. The measured S_{21} is depicted in Figure 14A which clearly indicates that the O-CSRR configuration shows weak resonance whereas the I-CSRR shows the prominent resonance behavior for $W_1/a > 1$. The good agreement between the simulated and

measured result indicate with the simulation (refer Figure 2). In order to get the confidence, one more set of the S_{21} data is measured corresponding to the $W_1/a > 1$ for $a = 2.3$ mm with keeping all other parameters same as mentioned above. The fabricated prototypes along with their S_{21} parameter response are shown in Figure 14B. This plot also shows the similar behavior as that of Figure 14A, that is, the ICSRR structure produces the good insertion loss unlikely the OCSRR structure for $W_1/a > 1$. Therefore, it can now be ascertained that the ICSRR structures proves to be viable choice over its OCSRR counterpart for design of high frequency resonators where usually size of resonators becomes relatively smaller than that of the width of the microstrip line, namely, $W_1/a > 1$ (Figure 14).

Finally, the few salient features of the OCSRR and ICSRR structures may list as follows:

1. The OCSRR structure and ICSRR structure produces the nearly similar rejection capability when $W_1/a < 1$ where, the ICSRR structure provides slightly improved rejection capability and 3-dB fractional bandwidth owing to its orientation relative to the microstrip line.
2. The ICSRR structures may be termed as the cross-polarized structure as these structures employs the electric as well as magnetic coupling with the host microstrip line. On contrary, the OCSRR structures may be termed as the copolarized structure as these structures only employs the pure electric coupling and hence these structure results to the overall symmetric device unlikely the asymmetric ICSRR counterpart.
3. The OCSRR structure produces the symmetric transmission coefficient phase response than that of the asymmetric phase response associated with the ICSRR topology.

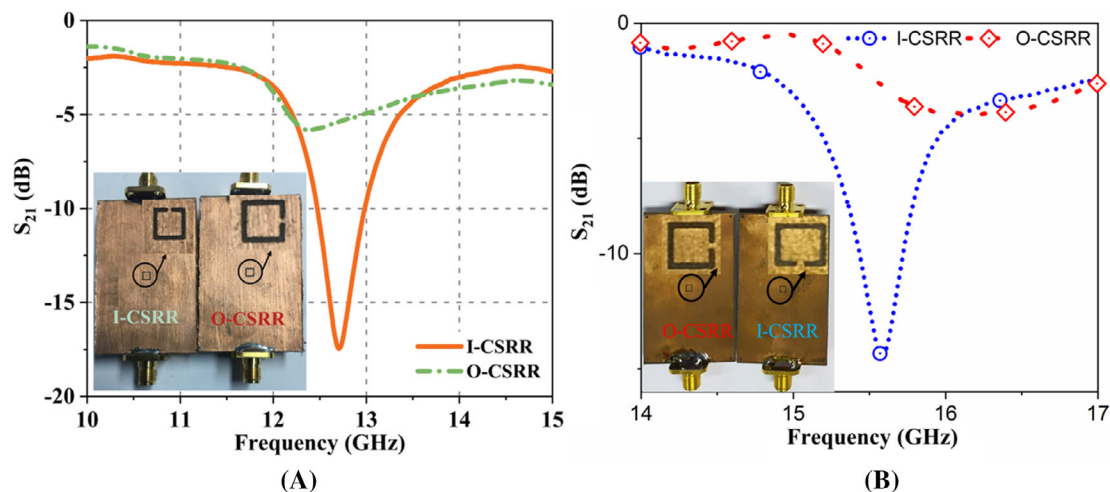




FIGURE 14 Measured S_{21} along with fabricated prototypes with $W_1/a > 1$, for (A) $a = 2.7$ mm, (B) $a = 2.3$ mm

4. The asymmetric phase response of the cross-polarized ICSRR topology enables to design the phase control circuit and system. The cross-polarization feature of the ICSRR topology proves to be viable option to excite it at relatively higher operating frequency than that of the polarized OCSRR topology for $W_1/a > 1$.
5. For $W_1/a > 1$, the ICSRR structure may produces the significant insertion loss as compared to poor insertion loss associated with the OCSRR structure and hence the compact high frequency circuits including the dielectric sensor can be designed using the ICSRR structures than that of the OCSRR structures where usually the condition $W_1/a > 1$ prevails.

4 | CONCLUSION

In this article, we have investigated the effect of orientation and relative size of microstrip coupled CSRR on its resonance. From the detailed analysis, it has been concluded that when the size of CSRR has been kept smaller than the host line, only the I-CSRR configuration show prominent resonance behavior due to the cross-polarization effect. In this case, the CSRR has been excited through mixed coupling, where the magnetic coupling dominates over the electric coupling. However, when the size of CSRR has been kept relatively larger than the width of the host line, the excitation of the CSRR is independent of its orientation. The investigation provided in this article could be useful to design the metamaterial-inspired microwave circuits (filters, sensors) and antennas in the higher frequency regime, where the relative size of CSRR is usually smaller. It has also shown that the proposed I-CSRR topology possesses the high frequency (15.6 GHz) dielectric sensing capability due to the presence of strong rejection even for the $W_1/a > 1$ unlikely the conventional O-CSRR topology.

ORCID

Nilesh K. Tiwari  <https://orcid.org/0000-0003-2582-0286>
Abhishek Sharma  <https://orcid.org/0000-0001-8026-9752>

REFERENCES

1. Marques R, Martin F, Sorolla M. *Metamaterials with Negative Parameters: Theory, Design, and Microwave Applications*. New Jersey: John Wiley & Sons; 2011.
2. Bonache J, Gil M, Gil I, Garcia-Garcia J, Martin F. On the electrical characteristics of complementary metamaterial resonators. *IEEE Microw Wirel Compon Lett*. 2006;16(10):543-545.
3. Falcone F, Lopetegi T, Baena JD, Marques R, Martin F, Sorolla M. Effective negative-stopband microstrip lines based on complementary split ring resonators. *IEEE Microw Wirel Compon Lett*. 2004;14(6):280-282.
4. Su L, Mata-Contreras J, Velez P, Martin F. Splitter/combiner microstrip sections loaded with pairs of complementary split ring resonators (CSRRs): Modeling and optimization for differential sensing applications. *IEEE Trans Microw Theory Tech*. 2016;64(12):4362-4370.
5. Tiwari NK, Singh SP, Akhtar MJ. Novel improved sensitivity planar microwave probe for adulteration detection in edible oils. *IEEE Microw Wirel Compon Lett*. 2018;1-3.
6. Sarkar D, Saurav K, Srivastava KV. Four-element array of complementary split-ring resonator loaded printed directive dipoles for triple band applications. *Electron Lett*. 2016;52(10):785-786.
7. Saraswat K, Harish AR. Dual-band CP coplanar waveguide-fed split-ring resonator-loaded G-shaped slot antenna with wide-frequency ratio. *IET Microw Antennas Propag*. 2018;12(12):1920-1925.
8. Marques R, Mesa F, Martel J, Medina F. Comparative analysis of edge- and broadside- coupled split ring resonators for metamaterial design—theory and experiments. *IEEE Trans Antennas Propag*. 2003;51(10):2572-2581.
9. Baena JD, Bonache J, Martin F, et al. Equivalent-circuit models for split-ring resonators and complementary split-ring resonators coupled to planar transmission lines. *IEEE Trans Microw Theory Tech*. 2005;53(4):1451-1461.
10. Duran-Sindreu M, Naqui J, Paredes F, Bonache J, Martin F. Electrically small resonators for planar metamaterial, microwave circuit and antenna design: a comparative analysis. *Appl Sci*. 2012;2(2):375-395.
11. Naqui J, Duran-Sindreu M, Martin F. Modeling split-ring resonator (SRR) and complementary split-ring resonator (CSRR) loaded transmission lines exhibiting cross-polarization effects. *IEEE Antennas Wirel Propag Lett*. 2013;12:178-181.
12. Mesa F, Jackson DR. The danger of high-frequency spurious effects on wide microstrip line. *IEEE Trans Microw Theory Tech*. 2002;50(12):2679-2689.

AUTHOR BIOGRAPHIES



Nilesh K. Tiwari (S'15) is with the Department of Electrical Engineering, IIT Kanpur, Kanpur 208016, India. He is currently pursuing the PhD degree at IIT Kanpur, Kanpur, India.



Abhishek Sharma received the BTech degree in electronics and communication and engineering from Shri Mata Vaishno Devi University, Jammu, India, in 2010, the MTech degree from AIT, New Delhi, India, in 2013 and the PhD from IIT Kanpur, Kanpur, India, in 2019. He is currently working as a postdoctoral fellow in the department of electronic engineering at City University of Hong Kong. His current research interests include Huygens' metasurface, bianisotropic metasurface, electromagnetic

theory, flat optics, dielectric resonator antennas, MIMO antennas and leaky wave antennas. He has authored/coauthored 20 peer-reviewed journal papers and 25 international conferences.



Surya P. Singh (S'13) is currently with IIT Kanpur, Kanpur, India. He is also with the International Institute of Information Technology Bhubaneswar, Bhubaneswar, India.



M. J. Akhtar (S'99-M'03-SM'09) received the PhD degree in electrical engineering from the Otto-von-Guericke University of Magdeburg, Magdeburg, Germany, in 2003. He was a scientist with the Central Electronics Engineering Research Institute, Pilani, India, from 1994 to 1997, where he was involved in the design and development of high-power microwave tubes. In 2009, he joined the Department of Electrical Engineering, IIT Kanpur, Kanpur, India, where he is currently a professor. He has authored two books, two book chapters, and has authored or coauthored over 250 papers in various peer-reviewed international journals and conference proceedings.



Animesh Biswas received the MTech degree in microwave and radar engineering from the IIT Kharagpur, India, in 1982, and the PhD degree in electrical engineering from the IIT Delhi, India, in 1989. From 1989 to 1990, he was a

postdoctoral fellow with Oregon State University, where he was involved in characterizing multi-conductor lines in layered medium. He is currently a professor with the Department of Electrical Engineering, IIT Kanpur, India. He has served as a technical consultant for M/S COMDEV Europe, and was involved in development of multimode DR filters and diplexers. His current research includes modeling of microwaves circuits, RF integrated circuits (RFICs), and numerical methods for solving electromagnetic problems. He has authored or coauthored over 195 papers in various peer-reviewed international journals and conference proceedings. He is a fellow of the Institution of Electronics and Telecommunication Engineers, India and senior member of IEEE, USA.

How to cite this article: Tiwari NK, Sharma A, Singh SP, Akhtar MJ, Biswas A. Novel analysis of the size and orientation dependent resonance phenomenon of the microstrip line coupled complementary split-ring resonator. *Int J RF Microw Comput Aided Eng.* 2020;30:e22038. <https://doi.org/10.1002/mmce.22038>